ELSEVIER

Contents lists available at ScienceDirect

Materials Today Sustainability

journal homepage: www.journals.elsevier.com/materials-today-sustainability





Development and evaluation of sustainable henequen fibre foams for thermal insulation

Qasim Shoaib ^a, Vaidurya Mukherjee ^a, Vasiliki Marmaridou ^a, Aleksei Sereda ^a, Peterasp Nawzar Satarawala ^a, Jose G. Carrillo ^b, Eral Bele ^a, ^b, ^{*}

- ^a Department of Mechanical Engineering, University College London, Torrington Place, WC1E 7JE, London, United Kingdom
- b Unidad de Materiales, Centro de Investigación Científica de Yucatán, Calle 43 No. 130 Col. Chuburná de Hidalgo, Mérida 97205, Yucatán, Mexico

ARTICLE INFO

Keywords: Materials circularity Sustainable manufacturing Natural fibre foams Thermal insulation Recycling Life cycle analysis

ABSTRACT

The increasing demand for sustainable thermal insulation materials stems from environmental concerns associated with conventional petroleum and mineral-based options, which exhibit high toxicity and global warming potential. While bio-based alternatives exist, they often present challenges related to chemically intensive processing, scalability, and cost-effectiveness. This study investigates the production of porous foams from lignocellulosic henequen fibres utilising a simple and scalable mechanical fibrillation process. Two distinct foam formulations were developed: one employing xanthan gum, a natural polysaccharide, as a binder to enhance structural integrity, and the other utilising borax, a natural mineral salt, to cross-link exposed cellulose in the fibrillated fibres. The resulting foams exhibited a highly porous structure with enhanced chemical and mechanical fibre interconnections. The xanthan gum-bound foam exhibited a thermal conductivity of 42 mW/m*K, an apparent density of 21 kg/m3, and a compressive stiffness of 56 kPa. The borax-crosslinked foam achieved a thermal conductivity of 43 mW/m*K, an apparent density of 11.5 kg/m3, and a compressive stiffness of 19 kPa. Notably, both foams demonstrated a limiting oxygen index of 29.5%, classifying them as self-extinguishing, despite the inherent flammability of the natural fibres. The xanthan gum-bound foam also maintained comparable physical and thermal properties after three recycling cycles. A cradle-to-gate life cycle assessment revealed significant reductions in toxicity and global warming potential compared to conventional insulation materials, specifically rigid polyurethane and glass wool. This research demonstrates the feasibility of utilising a straightforward fibrillation and template-forming process with abundant henequen fibres to produce sustainable insulation foams with good thermo-mechanical performance, improved fire safety, and a diminished environmental footprint.

1. Introduction

The building and construction sector is a major contributor to global energy consumption and greenhouse gas emissions. According to the United Nations Environment Programme, 37% of the global $\rm CO_2$ emissions in 2023 came from the building and construction sector [1]. Despite global commitments on decarbonisation by 2050, the gap between the current performance of the sector and the end-goal is widening [2]. Efforts to reduce building emissions have largely focused on the operation of buildings, such as heating, cooling and lighting. However, 11% of the global greenhouse gas emissions are attributed to the embodied carbon of building materials [3]. These emissions can be reduced by employing design strategies such as minimisation

of material use, improvement in circularity, and use of low-carbon or bio-based materials [1].

Thermal insulation materials are among the largest contributors to the embodied carbon of buildings, and it is estimated that low-carbon insulation could reduce the ${\rm CO}_2$ footprint of buildings by 9% [4]. Traditional insulation materials, such as mineral wool, glass wool and plastic foams, while effective in their thermal properties, often carry significant environmental drawbacks during all stages of their life cycle. For example, they cause increased biodiversity loss, water shortages and emission of toxic substances during manufacturing [5–7]. Moreover, since such materials are difficult to recycle, they are disposed in landfills, putting significant strain on waste management

E-mail addresses: qasim.shoaib.19@alumni.ucl.ac.uk (Q. Shoaib), vaidurya.mukherjee.19@alumni.ucl.ac.uk (V. Mukherjee), vasiliki.marmaridou.20@alumni.ucl.ac.uk (V. Marmaridou), aleksei.sereda.19@alumni.ucl.ac.uk (A. Sereda), peterasp.satarawala.19@alumni.ucl.ac.uk (P.N. Satarawala), jgcb@cicy.mx (J.G. Carrillo), e.bele@ucl.ac.uk (E. Bele).

https://doi.org/10.1016/j.mtsust.2025.101111

Received 25 December 2024; Received in revised form 7 March 2025; Accepted 3 April 2025 Available online 29 April 2025

^{*} Corresponding author.

systems - nearly 100 billion tonnes of waste are created annually from construction, renovation, and demolition operations [8]. Even when these materials are rescued and recycled, more than 35% of their waste is disposed of in landfills [9]. Thus, sustainable insulation options are urgently needed to mitigate these impacts, promote energy efficiency, and support the global shift towards green building standards.

Among the numerous eco-friendly insulation materials, natural fibre-based foams have emerged as promising candidates due to the wide availability of such fibres and their biodegradation potential. The main fibre sources for such foams are pulp (lignocellulosic) fibres, or cellulose obtained from fibre deep processing, such as cellulose nanofibres, microfibrillated cellulose, and nanocrystalline cellulose [10]. Examples of such fibre sources include sugarcane bagasse [11], wood fibres [12,13], bamboo fibres [14], pineapple leaves [15], soybeans [16, 17], and desert palms [18].

The manufacturing processes are of crucial importance, not only for the determination of thermophysical properties (i.e. functional competitiveness) of these materials, but also for the economic competitiveness and environmental performance. Broadly, they involve two stages: forming of the porous network template and drying. Template forming is generally achieved through two main methods: fibrillation and the use of binders. Fibrillation describes the entanglement of natural fibres by creating hairy fibres that have a complex assortment of branches and are suitable for mechanical interlocking. Chemical fibrillation techniques often use the same techniques for delignification, such as hydrolysis of $\rm H_2SO_4$ [19], and solutions of NaOH [20], however, the dangers of these chemicals and their environmental toxicities make them less suitable for environmentally beneficial scaled-up processes. Mechanical fibrillation, such as disk milling [21] is a strategy that has been successfully used to overcome the above disadvantages.

Drying processes are typically of three types: freeze drying, supercritical drying and ambient drying. Freeze drying [22-24], is very commonly used when cellulose is the primary base constituent of a foam, creating anisotropic structures [22] that have very effective thermal conductivities, in the order of 15-41 mW/m*K [10]. This, however, comes at a significant cost, as freeze drying is expensive, and thus the use of this method requires sacrificing the scalability of the end product. Supercritical drying involves a solvent exchange step, where the solvent entrapped within the pores of the wet foam is replaced by CO2 at pressures of 5-8 MPa [25,26]. Due to the need for extensive chemical treatments and specialised equipment to achieve the temperature and pressure requirements, the industrial scalability of this technique is challenging [27]. Oven or ambient drying is a common manufacturing process for such foams and is one most suitable for mass manufacture [28-30]. Its comparatively low energy to the alternatives, along with its simplicity, make it a strong choice for cellulose insulation that is geared toward mass manufacture rather than discovery.

The sustainability and scalability of these natural fibre foams ultimately depends on the primary source of fibres, and the energy consumption of the manufacturing processes. Often, the former receives little attention, however, it is an important consideration both in resource consumption (i.e., the proportion of fibres extracted from a given mass of organic material), and the time scale for the regeneration of the primary sources. Challenges related to deforestation and the uncertain availability of wood fibres make the sourcing and extraction of lignocellulosic fibres crucial for responsible industrial manufacturing [31].;

In this study, we target the above aims by the use of two simple and easily scalable manufacturing methods to manufacture low-density insulation foams from henequen fibres, a source that has not been considered previously in the literature of natural fibre foams. Henequen (agave fourcroydes) is native to Mexico and Guatemala [32], where it was cultivated extensively for the use of ropes before the advent of synthetic fibres; presently, its agricultural industry has been left with a surplus [32]. In industrial applications, the strong fibres are primarily used as reinforcement for polymer matrices, such as phenolic [33],

polypropylene [34] or epoxy [35] composites. In insulation applications, sisal fibres (a close relative) have been proposed as mixtures with gypsum [36], cement [37], or natural wool [38]. Investigations into the use of henequen in insulation foams, however, are exceedingly limited. Henequen is able to grow in environments that are semi-arid, with poor nutrition or even rocky, and exhibits better drought resistance than sisal [39].

This work describes the full process of manufacturing cellular solids from henequen fibres, evaluating their thermo-mechanical response and fire resistance. A simple blending approach is used for fibrillation of raw fibre bundles, and two methods are used for template forming: chemical cross-linking via borate ester bonds and mechanical crosslinking via Xanthan gum, a natural binder. All methods require simple equipment and are easily scalable, cost-effective, and of low energy intensity. This paper is organised as follows. First, the effect of the fibrillation treatment is reported on the fibre morphology and chemical composition. Next, the morphology and thermo-mechanical properties of the developed foams are presented and connected to the processing parameters through optimisation studies of two properties of interest: density and thermal conductivity. The fire resistance, a proof of concept demonstration of thermal insulation efficiency, and end-of-life pathways (recycling and biodegradation) are also presented. Finally, a life cycle assessment is conducted to contrast the environmental impacts with those of other synthetic and bio-based insulation materials.

Conventional methods for producing solid foams from natural fibres often necessitate chemical surface modification to enhance fibre-binder compatibility and mechanical interlocking [40,41]. This study presents a new approach, utilising mechanical fibrillation via high-shear blending in an aqueous medium. This process yields finer fibre structures with increased surface roughness, promoting enhanced chemical and mechanical bonding during foam drying. Furthermore, a critical advancement is the incorporation of borax, a naturally occurring mineral, to address the inherent flammability of lignocellulosic foams. Finally, the introduction of xanthan gum, a common food-grade polysaccharide, as a rheology modifier is demonstrated. In the wet foam matrix, xanthan gum increases viscosity, thereby improving structural integrity. Notably, while widely employed in other industries, the application of xanthan gum in stabilising and reinforcing natural fibre foams has not been exploited previously, representing a significant contribution of this research.

2. Materials and methods

2.1. Materials

The henequen fibres were obtained from Desfibradora La Lupita, located in Baca, Yucatan, Mexico. Their mean diameter, obtained from SEM was 381 \pm 6 μm (standard error with sample size of 102). Xanthan gum, procured from Sigma-Aldrich, was used as a stabiliser, sodium dodecyl sulfate (SDS), procured from APC Pure, was used as a surfactant, and sodium tetraborate, procured from HD Chemicals, was used as a flame retardant.

For better mechanical cross-linking, it was beneficial to separate the fibre bundles into finer ones via a simple fibrillation process. This was performed using a Suprills 2200 W blender. Optimal conditions for effective fibrillation were established after experimentation, using a water to fibre ratio of 100:1, and a mixing time of 6 min at 35,000 RPM. These conditions produced the highest aspect ratio and finest fibre diameters necessary for enhanced physical interlocking in foam formation.

2.2. Foaming methods

Two methods were used for foaming. The first used Xanthan gum as a stabiliser, sodium dodecyl sulfate (SDS) as a surfactant, sodium tetraborate as a flame retardant, and water; these are thereafter referred to as Xanthan foams. The wet foams were homogenised using an ONiLAB electric overhead stirrer for 15 min at 1000 RPM, poured into a bottomless silicone mould, and dried at 80°C for 12 h.

The second method had a composition similar to the above, but replaced the xanthan gum stabiliser with chemical cross-linking provided by the reaction of BO_3^{3-} anions (introduced through the dissolution of sodium tetraborate in water) and the -OH groups present in the cellulose fibres. This reaction results in borate ester bonds between adjacent cellulose fibres, and the resultant foams are thereafter referred to as Borate foams. A solution of fibrillated henequen fibres, sodium tetraborate and water was homogenised for 30 mins over a hot plate at 50 $^{\circ}\mathrm{C}$, adding SDS halfway through. The wet foam mixture was subsequently left to air dry for 24 h in bottomless silicon moulds.

The foams were dried in cylindrical moulds with a diameter of 5.5 cm and height of 3.5 cm. For the Xanthan foam, composition ratios were 2.5 g blended henequen fibres (5wt%), 0.25 g SDS (0.5wt%), 1 g borax (2wt%), 0.25 g xanthan gum (0.5wt%) and the remainder made of 46 ml water (92wt%). For the borate foam, the ratios were 0.75 g of blended henequen (1.5wt%), 1 g SDS (2wt%), 0.75 g borax (1.5wt%) and the remainder made of 47.5 ml water (95wt%). All wet foam mixtures had an initial mass of 50 g/specimen.

2.3. Testing equipment and methodology

Chemical composition changes in the henequen fibres during the fibrillation process were measured with a Nicolet iS50 Fourier Transform Infrared (FTIR) spectrometer. Surface morphology and dimensional changes during the fibrillation process were obtained using a Zeiss Gemini360 scanning electron microscope.

Tomographic scans to analyse the internal morphology and structure of the fibrous foams were performed using a Nikon XTH225 Micro Computed Tomography (CT) scanner, using a reflection anode at 75 kV and 327 μ A, comprising of 1032 projections, with a 1000 ms exposure time per projection and a voxel size of 50 x 50 μ m. The data was reconstructed using the embedded cone beam filtered back projection algorithms in CT Pro Nikon. Image analysis was performed using Avizo 3D (ThermoFisher Scientific).

Thermal conductivity measurements were conducted with an M1 HotDisk apparatus, which uses the transient plane source (TPS) technique. Thermal imaging of prototypes was conducted using a FLIR A35 Thermal Imaging Camera, an Etekcity IT Thermometer and a 150 W IR Lamp Cozion C9 C91075 to simulate heating conditions.

The compressive mechanical response of each foam was tested with an Instron 5969 universal tester, equipped with a 500 N load cell. Cylindrical specimens of 50 mm diameter and 35 mm height, obtained directly from the curing moulds, were compressed at a strain rate of $0.002~\rm s^{-1}$.

Finally, the environmental life cycle impact of the foams was analysed using Green Delta Nexus openLCA software with the Ecoinvent database. The process was adapted from ISO14040 [42], and the environmental impact methodology used were CML v4.8 2016 and ReCiPe 2016 v1.03, midpoint E [43].

3. Results

3.1. Effect of fibrillation on henequen fibre morphology

During the foaming process, fibre entanglement and mechanical interlocking occur, restricting relative displacement between adjacent fibres and enhancing structural stability. The degree of entanglement is proportional to fibre concentration and is further augmented by fibrillation. Fibrillation induces the dissociation of fibre bundles into smaller fibrils with surface-exposed microfibrils, thereby increasing the probability of inter-fibre entanglement and improving the dimensional stability of the resultant foam. The benefits of fibrillation in this context include increased air retention within the cured foam matrix and enhanced foam stiffness.

Fibrillation processes are common in the preparation of cellulose fibres for a variety of uses; the goal is to separate cellulose fibre bundles through wet abrasion. These processes also produces microfibrils on the fibre surfaces [44–46], which increase fibre entanglement and offer more support for the three-dimensional fibrous networks.

The morphology of henequen fibre bundles before and after fibrillation is shown in Fig. 1. An enlarged image of the section enclosed by the box in Fig. 1(a) is shown in Fig. 1(b) (rotated 180°). Untreated henequen fibres (Fig. 1(a) and (b)) are bundles of lignocellulosic microfibres [47,48], and their separation during fibrillation reduces the average fibre diameter from 381 \pm 6 (standard error with sample size of 102) μm to 21 \pm 1 (standard error with sample size of 120) μm . The latter is the smallest diameter achievable with this simple method, further increases in blending time or speed did not result in any further reduction in diameter.

The effect of blending on fibre length and diameter distribution is displayed in Fig. 2. In addition to the substantial decrease in diameter as mentioned above, the average fibre length also decreases, from 5.1 ± 0.2 cm (standard error with sample size of 100) to 2.9 ± 0.7 cm (standard error with sample size of 112). The narrow distribution width in fibre diameter post-blending indicates that the fibrillation technique is very effective in producing consistent cross-sections. By contrast, the wide distribution width in fibre length has been attributed in other studies to the large shear forces that act on the fibres when blended, which can peel away the surface of the fibres layer by layer with a certain degree of randomness [49] and cause the large variation observed.

Fibre entanglement is a stabilising mechanism for fibrous networks, as mechanical interlocking prevents relative displacement between adjacent fibres. This probability of interaction between fibres is increased with aspect ratio (length/diameter) [50]. The present results show clearly that the blending process increases the aspect ratio substantially, from 130 ± 3 to 1400 ± 92 , effectively increasing the probability for mechanical interlocking.

3.2. Effect of fibrillation on fibre composition

To understand the structural changes that occur in henequen fibres during the blending process, and to investigate the limiting factors that determine the minimum fibre diameter achieved with this process, a Fourier Transform Infrared (FTIR) spectroscopy analysis was conducted; the spectra of the fibres before and after blending are shown in Fig. 3. The spectra are normalised at 1020 cm⁻¹, corresponding to C-O bond stretching in cellulose and hemicellulose [51]. Peaks at 3300 cm⁻¹ and 900 cm⁻¹ correspond to the stretching of -OH groups and C-H bonds in cellulose, respectively. Both peaks are present in raw and blended henequen, indicating that the cellulose has remained after blending. The peaks at 1730 cm⁻¹ and 1227 cm⁻¹ correspond to the vibration of C=O and C-O bonds in acetyl groups, respectively, and are also present in each sample. These are both evidence of the presence of hemicellulose before and after blending [51]. The peak at approximately 1600 cm⁻¹, present in the raw henequen fibres, corresponds to aromatic skeletal vibrations and C=O bond stretching in lignin [51], and it is absent from the blended fibres. Similarly, other peaks at 1507 cm⁻¹ and 1421 cm⁻¹, also corresponding to the presence of lignin [51], are less prominent in the blended sample, indicating that the blending removes some lignin from henequen fibres. It is known that lignin and waxy substances are typically what binds the microfibres in the fibre bundle [47], thus, the process of blending effectively separates the microfibres. However, it does not separate further the microfibres, since the hemicellulose structure, which exists on the primary wall of the microfibres [48], does not break down through the shear forces generated from this mechanical process.

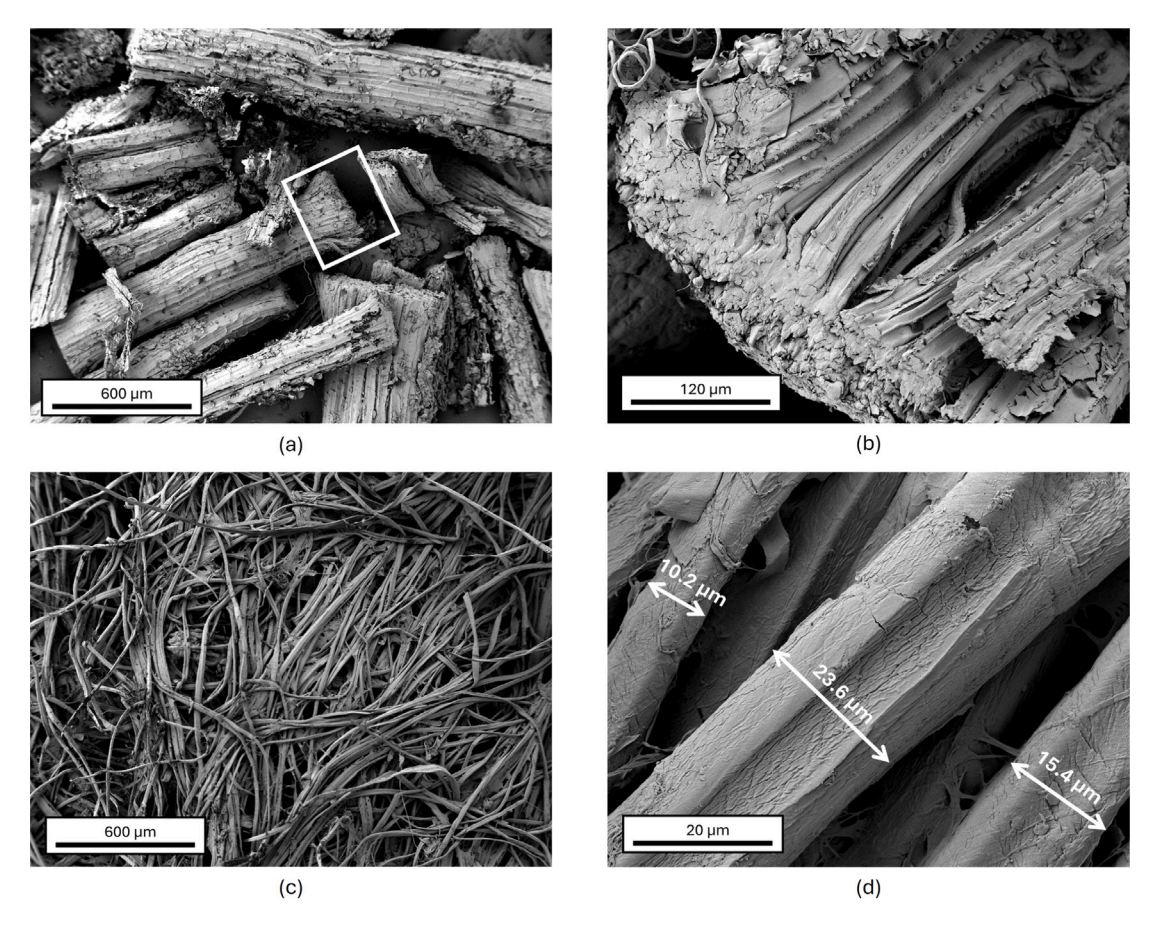


Fig. 1. SEM Images of raw henequen fibres (a) and (b) (showing a close-up of the boxed area in (a)), and blended henequen fibres (c) and (d).

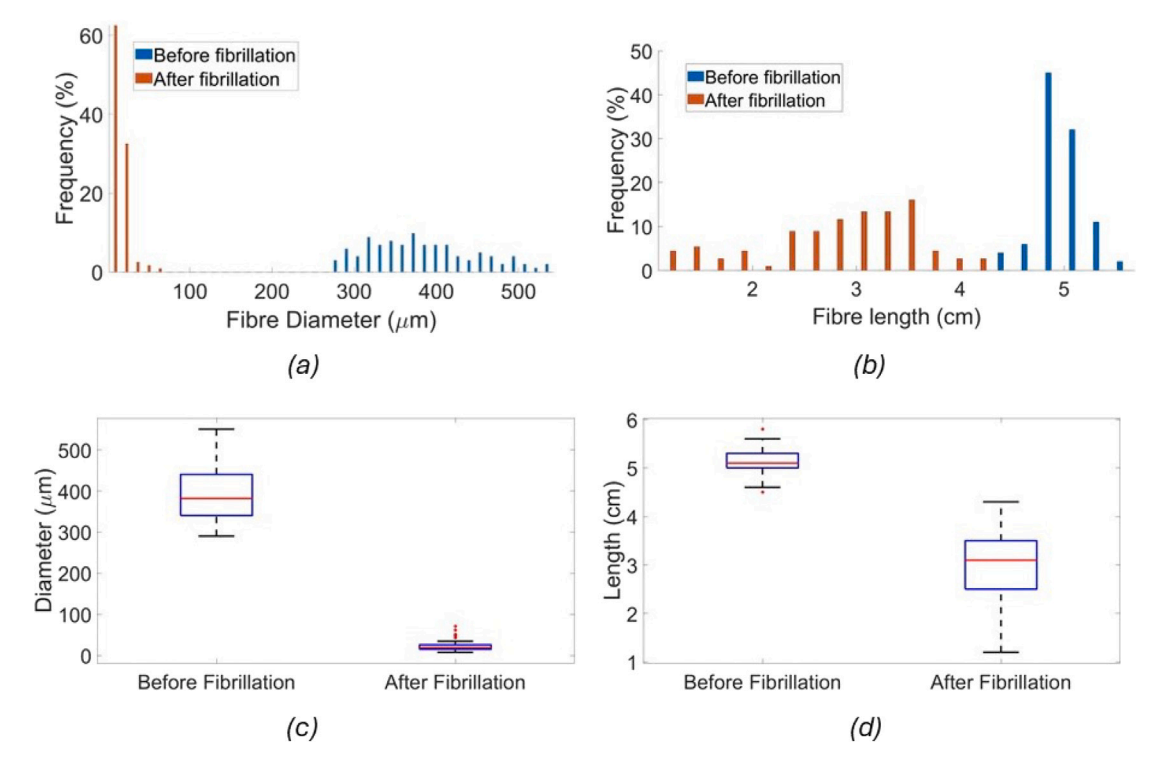


Fig. 2. Histograms and whisker plots of distribution of fibre length (a) and (c) and fibre diameter (b) and (d) before and after blending.

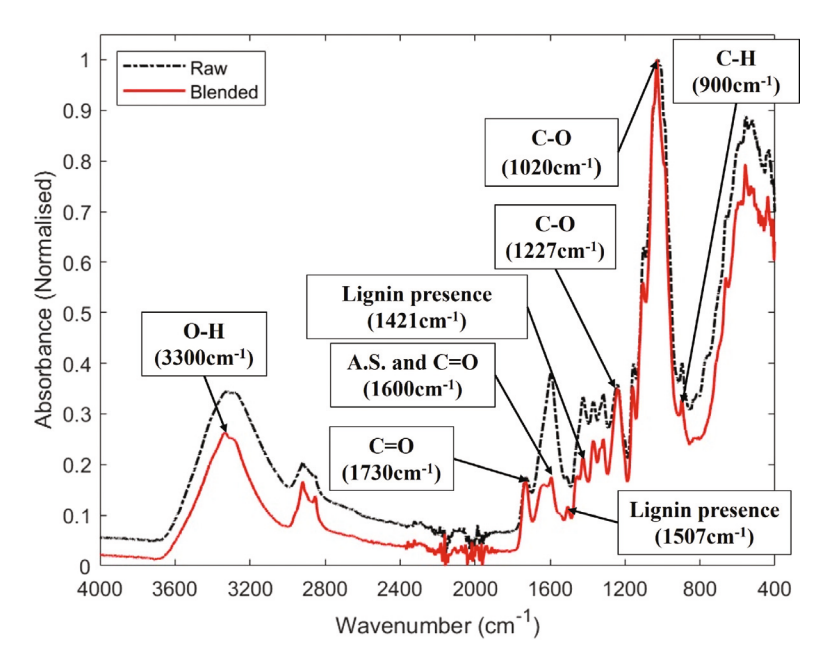


Fig. 3. FTIR of henequen fibre before and after blending.

3.3. Foam morphology

Fig. 4 shows typical morphologies of the Xanthan foam ((a), (c), (e), (g)) and Borate foam ((b), (d), (f), (h)). Optical micrographs and CT scans indicate a structure that is typical of fibrous networks composed of inter-twinned fibres in random orientations. The CT scans, shown in Fig. 4(c) and (d), were used to evaluate the macroscopic porosity, which was 94.4% for the Xanthan foam and 94.3% for the Borate foam.

The SEM micrographs elucidate the mechanisms of fibre interlocking. In the Xanthan foam (Fig. 4(e) and (g)) the henequen fibrils are physically adhered by the gum layer, which coats the surfaces of the fibres and creates a thin film in the intersecting areas. In the Borate foam, shown on Fig. 4(f) and (h), interactions are observed between the microfibre surfaces, even in the absence of an external binding agent. Fig. 4(h) showcases an example of the formation of new common surface interactions between individual fibres as a result of the chemical cross linking, to form new 'branched' junctions between adjacent microfibres. In both cases, these crosslinking mechanisms serve to prevent relative displacement between adjacent fibres and are compounded throughout the entire fibre network to ultimately stabilise the foam on a macroscopic level.

An important characteristic of porous fibre networks is the free distance between inter-fibre junctions, which characterises the effective pore size. The frequency distribution of the free fibre length was extracted from the CT scans and is shown in Fig. 5. The mean value of the free fibre length is 2.6 mm and 2.1 mm for the Xanthan and Borate foams, respectively. The median free length is 1.8 mm in both foams, indicating that there is a higher concentration of smaller pores relative to big pores in the structure, which is important to achieve a low thermal conductivity. Note that cellulose nanofibril aerogels often achieve free lengths in the order of nm- μ m [52], albeit through a more energy-intensive manufacturing process (freeze drying and supercritical drying) than that of the present study, and this morphology in turn accounts for very low thermal conductivity values, in the range of 15–41 mW/m*K [10].

Thermal insulation foams achieve their insulating capacity through the presence of a porous architecture. This porosity consists of discrete air (or gas) enclosures entrapped within the solid matrix. An increased number of cells generally correlates with enhanced thermal performance, attributed to the inherently low thermal conductivity of air [53]. Consequently, the high volume fraction of entrapped air within the developed foams contributes to thermal resistance through two primary mechanisms. Firstly, the foam's cellular morphology, characterised by a relatively uniform distribution of pores within the fibrous network, effectively mitigates convective heat transfer. Secondly, the low density of these foams significantly reduces conductive heat transfer through the solid phase. By minimising the solid material available for heat conduction, the foams effectively limit the transfer of thermal energy through the structural matrix.

3.4. Presence of borate cross-linking

The chemical cross-linking of henequen lignocellulosic fibres in the Borate foam is achieved through borate-ester bonds, and their formation was verified by FTIR. The spectra of untreated fibres (obtained before the addition of sodium tetraborate), and Borate foam fibres (obtained from the dry foam after the addition of sodium tetraborate) are shown in Fig. 6. The data is normalised at the common 1040 cm $^{-1}$ peak, characteristic of C–O bond stretching within the cellulosic structure [54,55].

The new peak observed at 1355-1430 cm⁻¹ corresponds to the asymmetric stretching mode of the new B-O-C bonds formed and is indicative of a successful reaction between the borate ion and the cellulosic fibres to form borate ester bonds [56-58]. The observed peak within this specific wavelength range aligns with the characteristic signature of B-O-C bond formation in cellulose networks, a phenomenon consistently reported in numerous studies investigating the application of borax in cellulose hydrogel systems [56-60]. This spectral evidence strongly suggests the establishment of chemical crosslinkages within the developed fibre network. Further corroboration of this chemical cross-linking mechanism is provided by the behaviour of control samples. Specifically, when a foam formulation identical to the borax-modified foam, but devoid of borax, was subjected to air drying, the resulting fibre network exhibited a pronounced structural collapse, accompanied by a subsequent loss of measurable structural rigidity. This stark contrast in structural integrity between the borax-modified and control foams serves as a compelling indicator of successful chemical cross-linking, thereby demonstrating its crucial role in stabilising and reinforcing the foam structure.

The peaks observed at 820 cm⁻¹ and 580–500 cm⁻¹ were identified to be residual borate and tetraborate, respectively, which remained as excess from the borax agent used in the procedure [58,61]. Finally, the

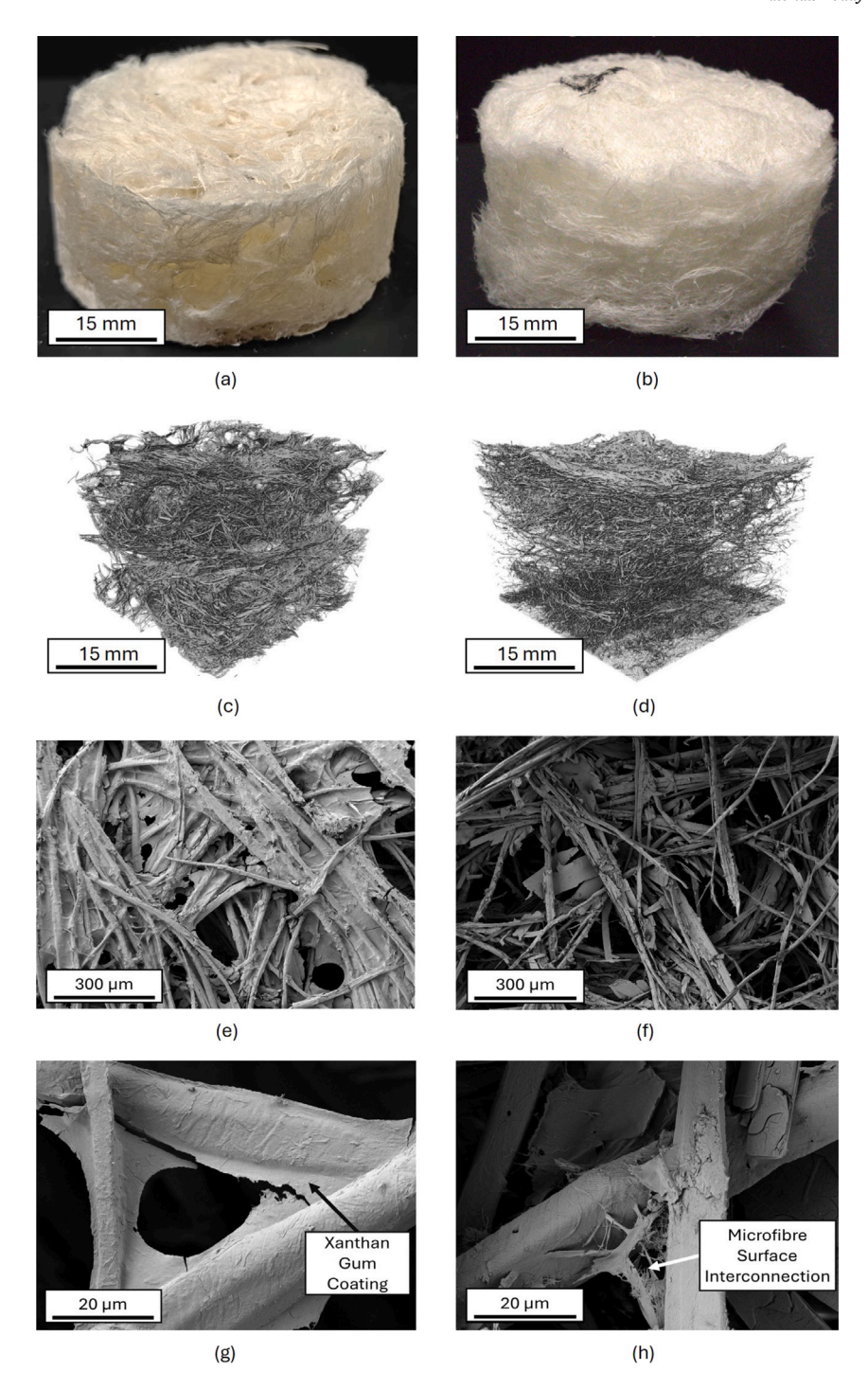


Fig. 4. Macroscopic images of Xanthan foam (a) and Borate foam (b), CT Scan images of Xanthan foam(c) and Borate foam(d), and SEM images of Xanthan foam (e), (g) and Borate foam (f), (h).

peak observed at $3400~\rm cm^{-1}$ represents free -OH groups within the cellulose molecular structure [57,58]. Although this peak did not diminish significantly, the dulling is indicative of some molecular interaction and alteration of these groups. This was expected due to the chemical interaction with the borate ion.

3.5. Compressive response

The compressive response of the optimised foam formulations outlined below is shown in Fig. 7 and indicates two distinct regimes: an initial elastic regime, followed gradually by strain stiffening. The

response is typical of fibrous networks, and the Xanthan foam shows clearly the two sub-regions of the initial deformation response: the small-strain linear regime due to fibre rearrangement [62] or bending [63], followed by a second regime controlled by fibre bending and buckling [63]. The densification regime occurs due to the internal geometrical constraints arising from the development of new fibre-fibre contacts at large strains [63,64].

The initial stiffness of the Xanthan and Borate foams is 56.4 kPa and 19.4 kPa, respectively. As expected, the mechanical bonding via the Xanthan gum in the fibre junctions increases both the stiffness and density of these foams compared to the chemical cross-linking achieved in the borate foams. However, both foams surpass the BS ISO 21844

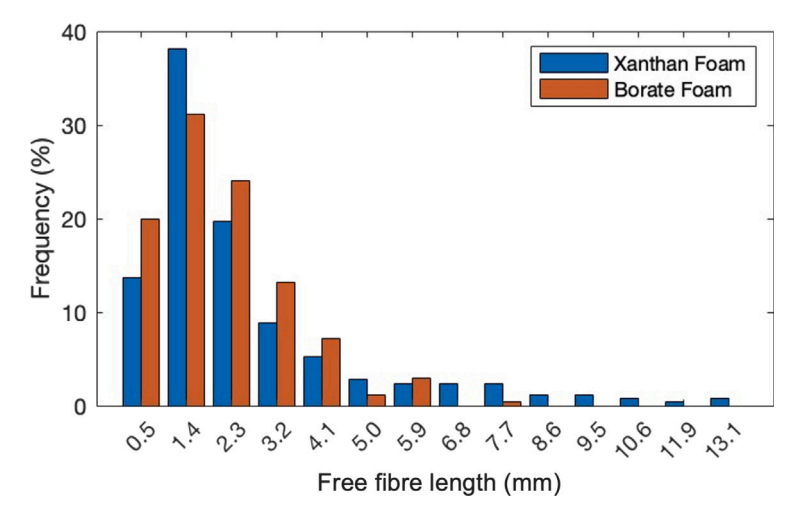


Fig. 5. Free length distributions of Xanthan and Borate foams.

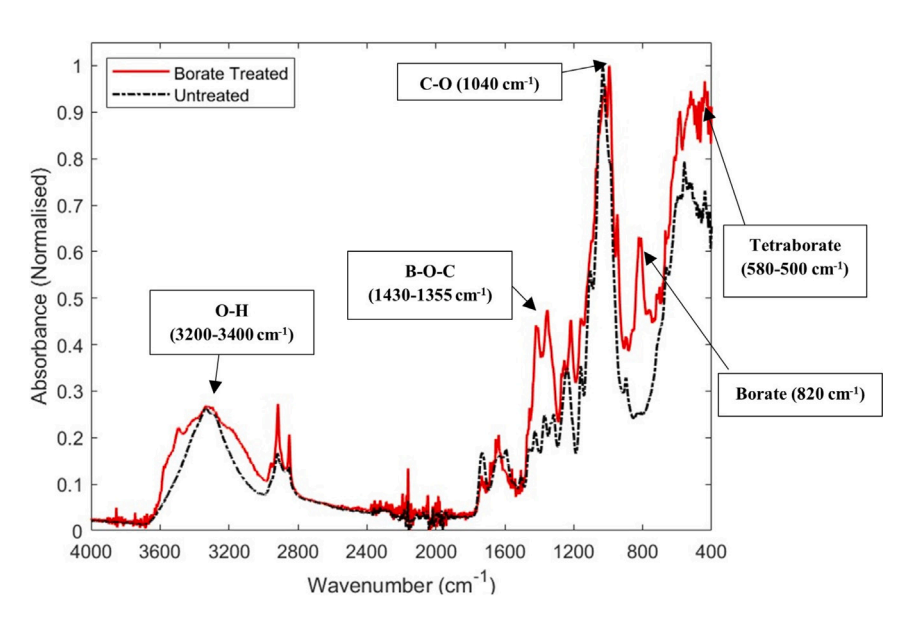


Fig. 6. FTIR spectra of borate foam and untreated blended fibres.

category 1 standard for cellulose insulation foams, 7 kPa (measured at 10% deformation) [65].

4. Discussion

4.1. Borate foam optimisation

To minimise the thermal conductivity of a foam structure, it is typically necessary to also minimise density. The borate foam design described here exploits the mechanisms of fibre entanglement and borate cross-linking in synergy to increase volumetric stability and minimise density. These stabilising mechanisms are influenced by the fibre and borate concentration in the wet foam mixture and in turn, determine the properties of interest in insulation materials: density and thermal conductivity.

The fibre concentration in the wet foam was adjusted incrementally, and in each case, the concentration of borate salt was maintained at a 1:1 mass ratio to fibre. The fibre concentration has a strong influence on the density and conductivity of the final dry foam, as shown in Fig. 8(a), with minima in both properties at a fibre concentration of 1.5 (wt%). Below this critical concentration, foam collapse was observed. At higher concentrations, the foam maintained volumetric stability upon drying, but the density and thermal conductivity increased.

The influence of borax concentration on density and thermal conductivity was evaluated for foams with the critical fibre concentration determined above; the results are presented in Fig. 8(b). A point of minimum density was again observed, below which the dry volume reduced and increased density, and above which volume remained approximately consistent but mass increased. Indeed, a foam was created even in the absence of the borate agent, but it displayed greater shrinkage on drying and an overall reduction in volume compared to those with borate addition. The minimum density was $10.7~{\rm kg/m^3}$, achieved at a borax-fibre ratio of 50 wt%. Thermal conductivity is less sensitive to borate concentration: minima were observed at borax-fibre mass ratios of 50 wt% and 100 wt%, with values of $0.043~{\rm W/m^*K}$ and $0.044~{\rm W/m^*K}$ for thermal conductivity, respectively, at apparent densities of $10.7~{\rm kg/m^3}$ and $11.5~{\rm kg/m^3}$, respectively.

The overall trend may be explained by the limited availability of reaction sites for a cross-linking mechanism to occur. Above a critical point of borate addition, these reaction sites are exhausted, and borate salt remains as excess within the wet foam mixture, not contributing to additional cross-linking and volumetric stabilisation of the foam and instead draining out with the aqueous phase upon drying or remaining as dry mass in the final foam. Importantly, the inclusion of the borate agent results in an increase in volumetric stability, thus providing

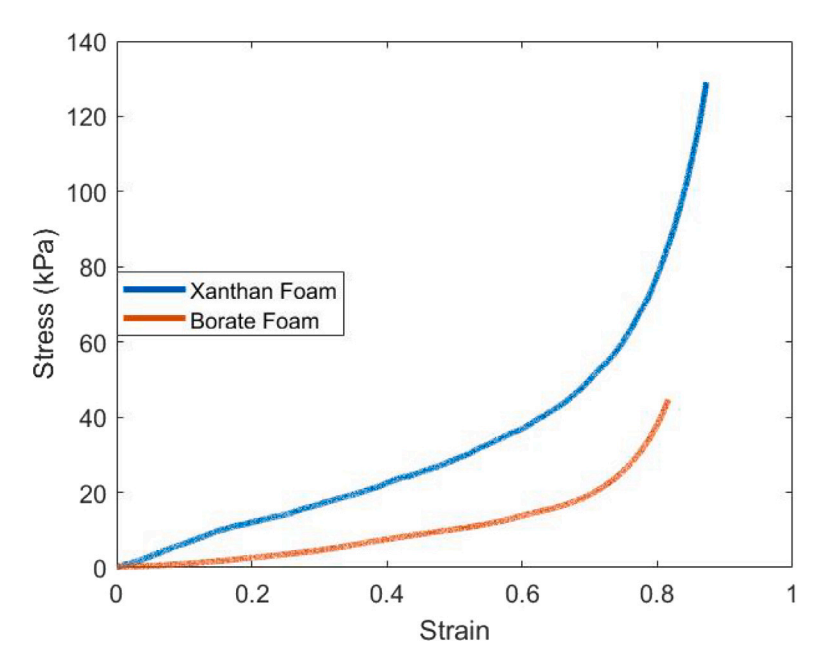


Fig. 7. Stress-strain graphs for Xanthan and Borate foams.

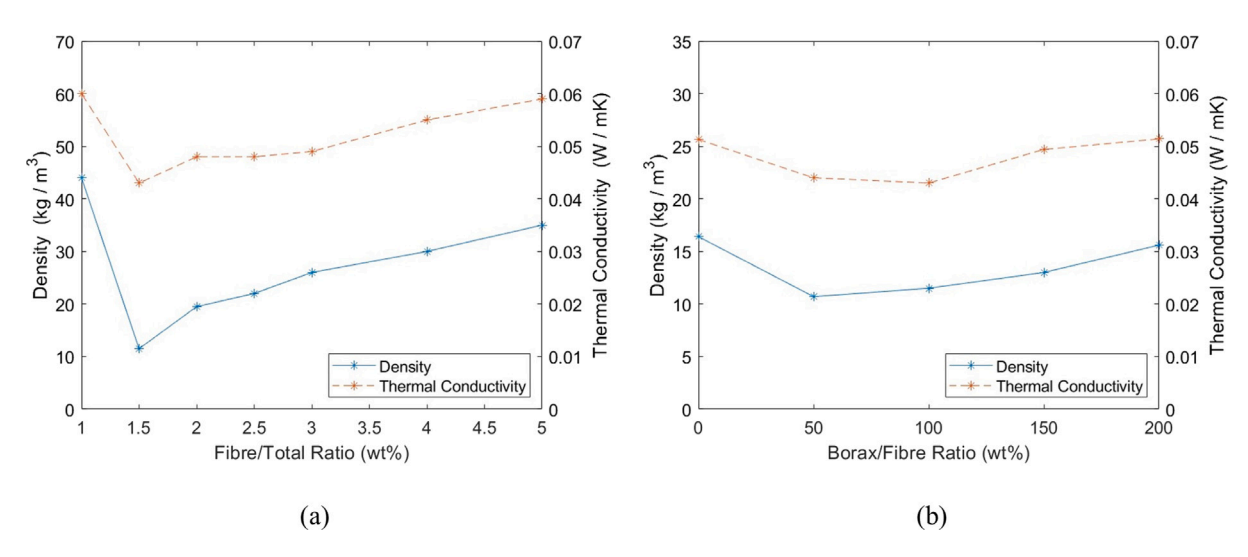


Fig. 8. (a) Plot of foam density and thermal conductivity against weight ratio of fibre/total, (b) Plot of density and thermal conductivity against borate/fibre ratio by weight.

evidence for a successful cross-linking mechanism with the cellulosic fibres.

4.2. Xanthan foam optimisation

Pore formations in insulation foams are beneficial to exploit the low thermal conductivity of air, but coalescence can lead to foam collapse. Stabilisers, such as the Xanthan gum of this study, are a means of remedying the collapse by providing rigidity to the end product. Optimisation studies were also conducted for this manufacturing technique; the effect of fibre and Xanthan gum concentration on apparent density and thermal conductivity is shown in Fig. 9.

The practical range of the henequen fibre concentration in the wet foam solution is 1–10 wt%. At lower values of fibre concentration, a foam failed to be produced due to the insufficient fibre content to create a stable porous network. An increase in fibre content generally corresponds to a larger apparent density, with eventual collapse of the porous network at large fibre concentrations. The dependence of thermal conductivity on fibre concentration qualitatively follows that

of the apparent density, as expected from the air entrapment (porosity) of the networks.

The effect of the fibre/Xanthan ratio is more complex. Generally, increasing this ratio decreases the thermal conductivity and density of the dry foams due to the reduced viscosity of the liquid solution, which, in turn, aids draining without collapse of the fibrous network. However, local optima exist, which balance, on one hand, the stabilisation of the fibrous network by the gum binder and, on the other, sufficiently low viscosity to facilitate drainage without collapse. Minimum thermal conductivity of 0.042 W/m*K and density of 21 kg/m³, was obtained at a fibre concentration of 5 wt% and fibre/xanthan ratio of 10:1.

4.3. Fire resistance

For both foams, the natural fire resistance of boron, present in borates, was utilised by adding borax to each foam to deliver each with a suitable level of flame retardance, a necessary property for insulation foams. Borax is a natural sodium salt that is very commonly used with cellulose insulation. It contains boron, which actively releases water when burnt, and this reaction promotes char formation, thus restricting

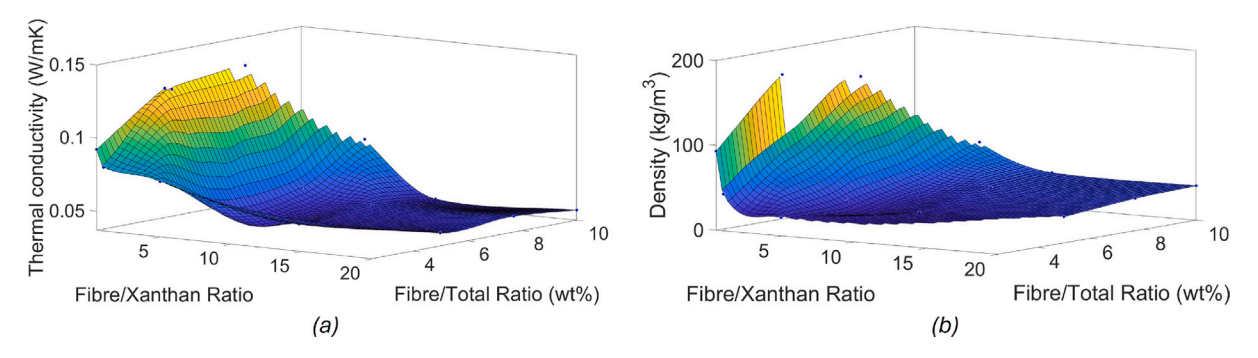


Fig. 9. Effect of Henequen fibre concentration and Fibre/Xanthan ratio on the thermal conductivity (a), and density (b) of Xanthan-stabilised foams.

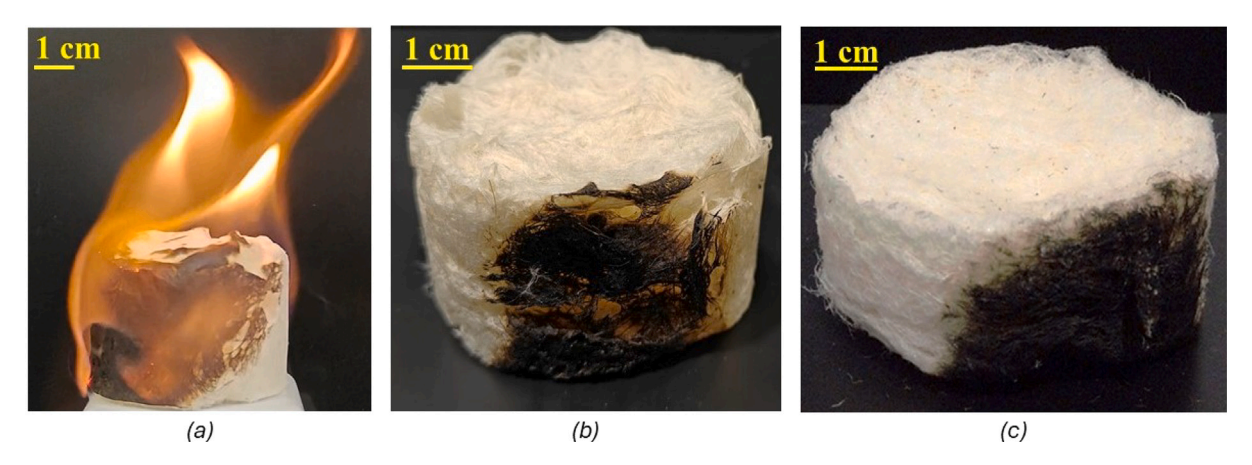


Fig. 10. (a) Xanthan foam with no borax, (b) Xanthan foam with borax after burning for 30 s, (c) Borate foam after burning for 30 s.

damage only to where a foam is burnt [66]. A second benefit is that borax homogenises well within the wet foam mixture, thus providing its flame retardant properties throughout the foam. This expounds its use in cellulose foams since its homogenisation capabilities allow for a counteraction of the natural flammability of cellulose-based materials.

Fig. 10 visually depicts basic flame retardance tests for the Xanthan and Borate foams. In (b) and (c), it can be seen that both foams self-extinguish after flame exposure of 30 s, with surface char formation cutting off the oxygen supply to the flame and preventing further spread. By contrast, a Xanthan foam without the addition of borax indicates high flammability, shown in Fig. 10(a), at the same time after flame exposure.

Fig. 11 presents microstructural images elucidating the combustion behaviour of the foams, including pre-combustion morphology (a), post-combustion residue (b), the combustion boundary (c), and a macroscopic overview of the partially combusted specimen (d). The initial foam microstructure, characterised by a composite of macroscopic fibres and intricate microfibrous networks (a mesh of smaller, entangled fibres), transitions to a residual network of charred macrofibres following combustion. Notably, the macroscopic structural integrity is preserved post-combustion, despite a substantial loss of microfibrillation. Image (c) reveals a well-defined combustion front, indicating localised combustion. The presence of small flame tendrils near this boundary suggests localised regions of lower borate concentration, which serve as preferential pathways for flame propagation. The localised combustion volume is further demonstrated in (d). These observations collectively indicate a homogeneous distribution of borates in the volume of the foam, validating their efficacy in both impeding flame propagation and confining the combustion zone.

Flame retardancy was quantified by the Limiting Oxygen Index (LOI) method, according to ASTM D2863 [67], using a Stanton Redcroft FTA module. LOI values of > 20.95% are classified as 'slow burning' [68], and values of > 28% are classed as 'self extinguishing' [69,

70]. In both foams of this study, an LOI value of 29.5% was obtained, classifying them as 'self extinguishing'. Since the lignocellulosic fibres are generally flammable, it is significant to note the effectiveness of borax as a fire retardant in these classes of materials.

Although the LOI test and characterisation of the combustion mechanisms provide encouraging data, in the journey to the commercialisation and application of these materials in the construction industry, further testing can be performed to provide a comprehensive and standardised evaluation of their flame retardancy performance. An example of a typical fire rating test for building materials in the European Union is the Euroclass system, which assesses factors such as non-combustibility (ISO 1182), ignitability (ISO 11925-2), heat release upon combustion, smoke production, and the formation of burning droplets [71]. Materials are subsequently assigned a rating from A1 (non-combustible) to F (most flammable), following the European standard EN 13501-1 [72].

4.4. Thermal imaging

Validation of the effectiveness of the developed lignocellulosic foams as insulation materials can be provided via the proof-of-concept setup demonstrated in Fig. 12(a). A polypropylene box, of dimensions $115\times63\times175\,$ mm was insulated on one surface via panels of the two foams developed here, and a polyurethane (PU) foam of density $30~kg/m^3$ and coefficient of thermal conductivity 0.022 W/m*K. All insulation panels had dimensions $180\times120\times25\,$ mm and were placed 15~cm below a 150~W infrared heat lamp. The temperature distribution in this setup was measured until steady state with a FLIR A35 thermal imaging camera and validated at steady state with an Etekcity Lasergrip 774 infrared thermometer. The temperature of the box without an insulation panel was also measured as a control setup.

The steady-state temperature distribution of the setup with the Xanthan foam panel is shown in Fig. 12(b). It is clear that the insulation

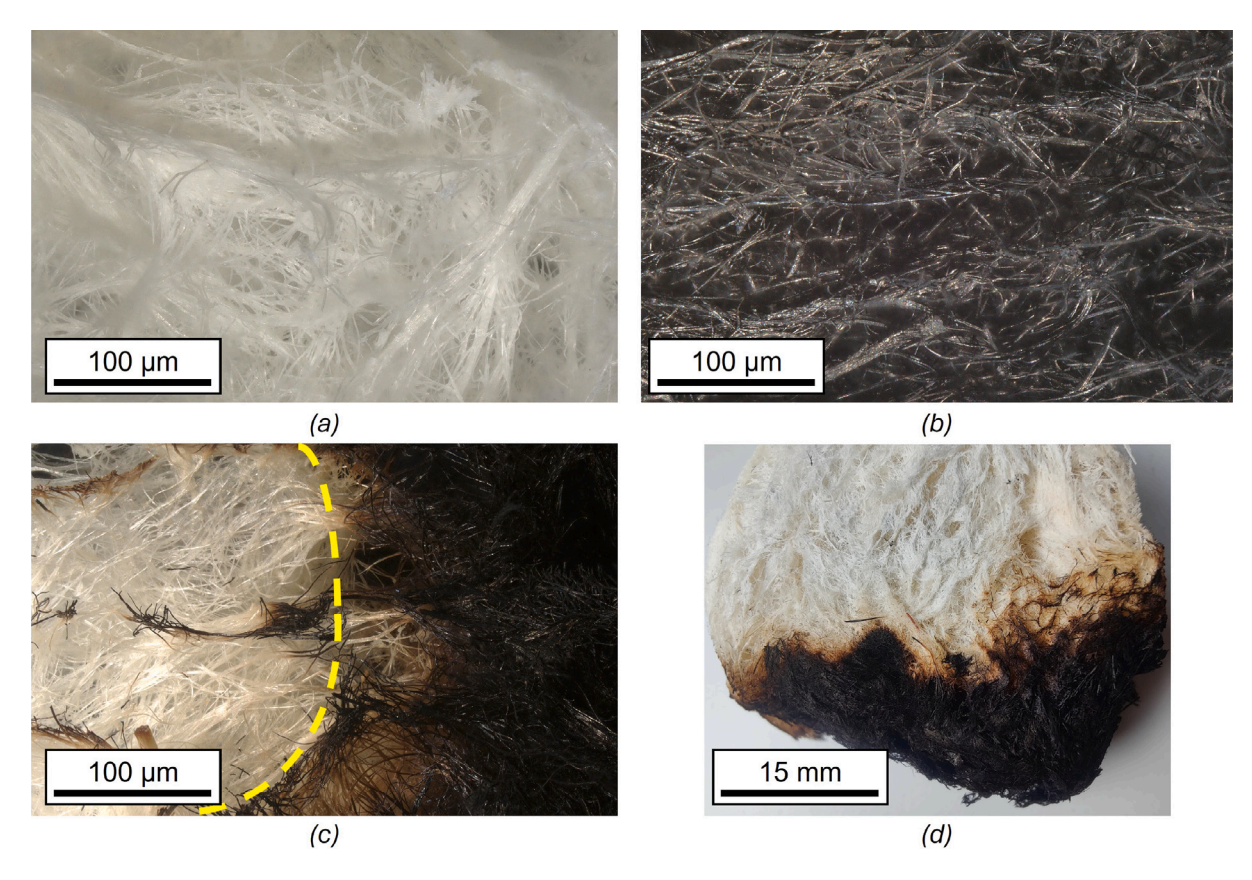


Fig. 11. (a) Xanthan foam before combustion, (b) Xanthan foam after combustion, (c) Depiction of boundary between combusted foam and unburnt regions, (d) Macroscopic view of burn line boundary.

panel displays a significant thermal gradient, indicating its suitability as an insulation material.

The evolution of temperature in the box (T_{in}) and the outer surface of the insulation panels (T_{out}) is shown in Fig. 12(c). To compare each of the materials fairly, a power level for each was chosen where the temperature on the top surface was constant, at 52.5 °C. At these power levels, the temperatures for the foam's surface (outer temperature) and inside the box (inner temperature) are measured as plotted on Fig. 12(c). A control temperature is also plotted to measure the temperature in the box without any foam. This temperature continually increases as expected. The temperatures on top of each foam reach a steady state at different times. For the heat that is transmitted through to the box, the Xanthan foam and PU have incredibly similar temperatures, whereas the borate foam displays a marginally higher temperature.

Two main conclusions are noted. First, steady state, defined as $d(T_{out}-T_{in})/dt<1$ °C/min is reached relatively quickly in all three panels, at 35 mins, 55 mins, 50 mins for the Xanthan, Borate, and PU foam respectively. Second, the steady state temperature difference $\Delta T=T_{out}-T_{in}$, an indicator of the insulation efficiency in this heat flux setting, is similar in all three materials, at 26.5 °C, 25.5 °C, 29.2 °C for Xanthan, Borate and PU foam, respectively. The above results are an encouraging indication of the competitive thermal insulation capability of the developed lignocellulosic foams.

4.5. Comparison with other porous materials and technical compliance

The developed materials are intended for thermal insulation applications within building envelopes, encompassing walls, roofs, and floors, to enhance energy efficiency and indoor environmental quality. These bio-based foams offer a sustainable alternative to conventional fossil-fuel-derived insulation materials, such as polyurethane (PUR) foam, extruded polystyrene (XPS), and expanded polystyrene (EPS), as

well as mineral-based options like fibreglass and rock wool, thereby reducing environmental impact. Furthermore, they expand the range of sustainable foam options available for construction. While low-density porous materials derived from fossil fuels and minerals are also utilised in soundproofing and industrial insulation, including piping systems, ductwork, storage tanks, and silos, future investigations can explore the suitability of these sustainable foams for such applications.

The newly developed Borate and Xanthan foams exhibit lower densities compared to many similar lignocellulosic fibrous insulation materials and most fossil fuel-based insulation materials, which all fall under the general category of commercial insulation products, as shown in Fig. 13. The threshold for commercial thermal insulation products (0.05 W/m*K) is based on an average of available data sets, according to [81], and is satisfied by the materials developed in this study. The reduced density suggests lower material intensity and decreased resource depletion, measured below via a Life Cycle Assessment. The thermal performance of the developed materials is comparable to that of other bio-based insulation options, however, at a lower density. While mineral wool and traditional fossil fuel-based insulation such as glass wool and EPS offer lower thermal conductivity values, the hereindeveloped foams show promise as a resource-efficient alternative for sustainable building practices.

A key innovation of the developed foams is their inherent flame retardancy, achieved through the incorporation of borax. This characteristic contrasts significantly with conventional foam materials. Polyurethane (PUR) and expanded polystyrene (EPS) foams are classified as highly flammable, while mineral-based foams, such as rock and mineral wool, are non-combustible. Untreated plant-based foams are generally susceptible to combustion. While some commercial bio-based foams, such as those derived from kenaf and wood fibre in the graph of Fig. 13, incorporate flame-retardant additives [76–78], the borax-modified foams presented herein offer an inherently flame-retardant alternative.

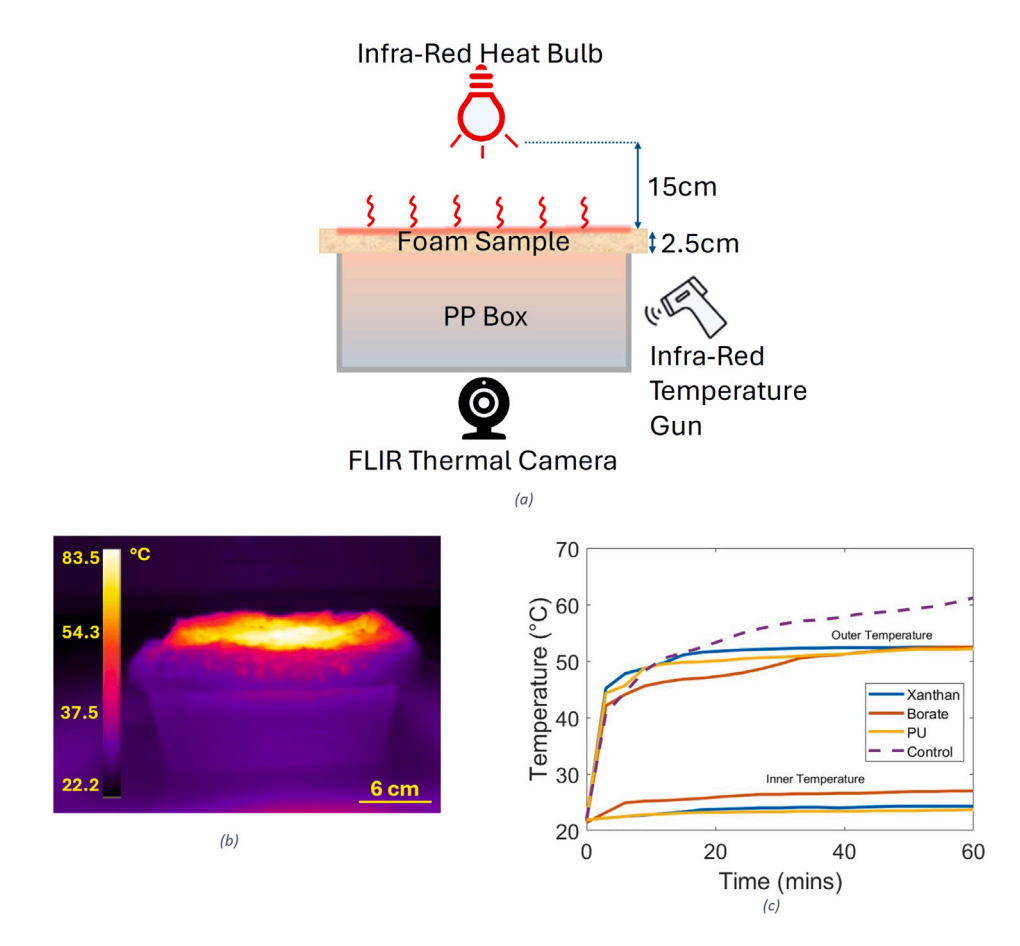


Fig. 12. (a) Schematic of the proof-of-concept experimental setup of thermal insulation panels, (b) Temperature distribution of the setup with Xanthan foam panel at steady state, (c) Temperature evolution at the outer surface of the insulation panel and inner box.

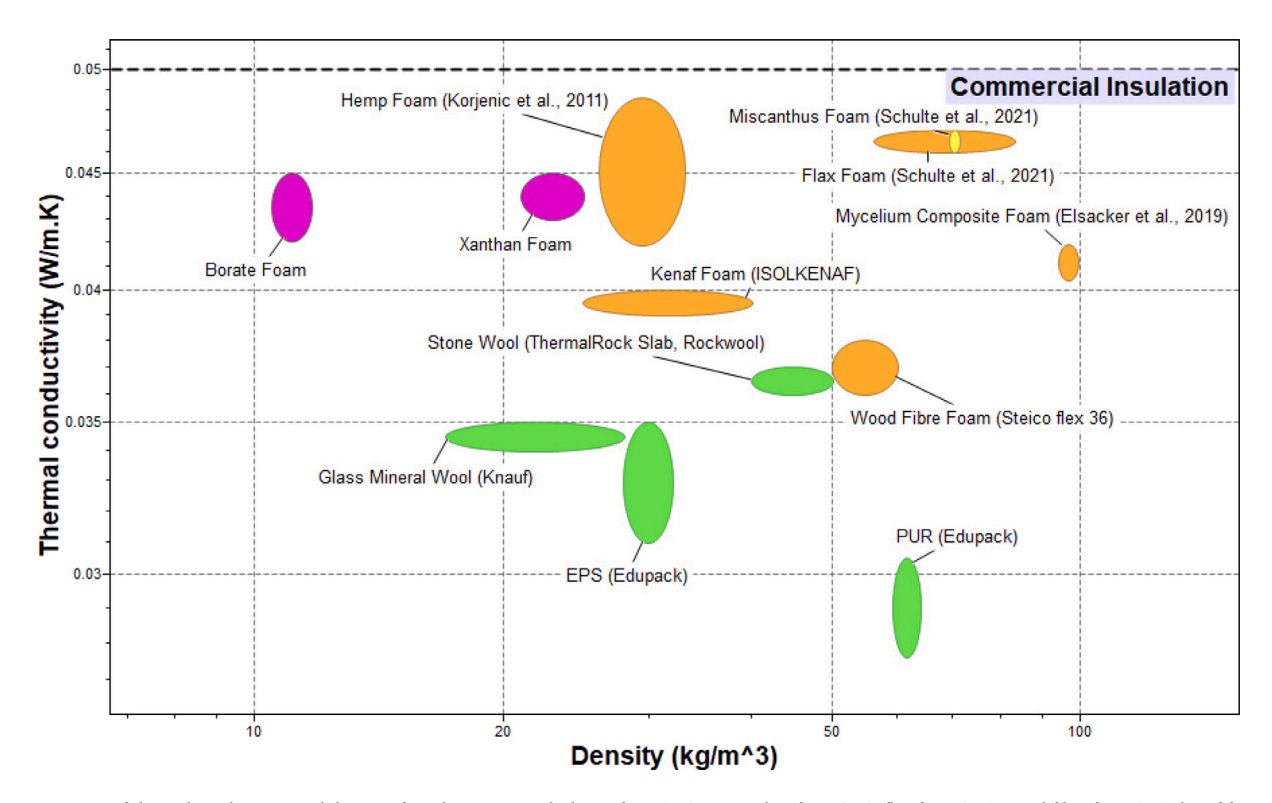


Fig. 13. Comparison of thermal conductivity and density of insulation materials: hemp foam [73], miscanthus foam [74], flax foam [74], wood fibre foam [75], kenaf foam [76,77], stone wool [78], glass mineral wool [79], mycelium composite [80].

Compared to porous materials fabricated via chemical cross-linking and ambient drying of natural fibres, the Borate foam exhibits lower stiffness (56 kPa compared to 6–40 MPa in the previous foams) [82]. However, these mechanical properties are achieved at a substantially lower density (11.5 kg/m³) relative to comparable foams (90–210 kg/m³) while maintaining a similar thermal conductivity range (0.044–0.049 W/m*K), resulting in enhanced weight-specific insulation performance [27]. The Xanthan foam, produced through mechanical interlocking and oven-drying at 80 °C, demonstrates a lower apparent density (21 kg/m³) compared to foams manufactured by similar methods (34–75 kg/m³) [83]. Its stiffness and thermal conductivity fall within the ranges reported for these comparable foams (0.0128–0.1359 MPa and 0.0385–0.0421 W/m*K, respectively) [83].

In comparison to process-intensive cellulose nanofibre (CNF) foams manufactured via oven drying, the developed foams exhibit lower thermal conductivity (0.0486 W/m*K for CNF foams) at a comparable density (12–22 kg/m³ for CNF foams) and stiffness (0.02–1.5 MPa for CNF foams) [84]. Finally, when compared to CNF foams manufactured using microwave drying, the henequen-based foams demonstrate lower density and thermal conductivity (100–200 kg/m³ and 0.046 W/m*K, respectively) [85]. This indicates superior performance as a lightweight insulation material.

In accordance with the technical performance requirements of BS ISO 2184 for cellulose foam thermal insulation [65], the Xanthan foam exhibits characteristics closely aligned with Category I, which specifies a density exceeding 20 kg/m³ and a thermal conductivity below 0.040 W/m*K. Notably, while meeting the density criterion, its thermal conductivity is within 5% of the thermal conductivity limit. The Borax foam also satisfies this categorisation, albeit at a lower apparent density. Both foam types fulfill the compressive strength requirement of Category I materials (above 7 kPa). It is essential to acknowledge that BS ISO 2184 pertains to closed-cell foams composed of cellulose-starch ingredients and composed of a fine, uniform, independent air bubble morphology. Consequently, it is not directly applicable to the open-cell. lignocellulosic fibre-based materials developed herein. Nevertheless, the proximity of the thermomechanical properties of the current materials to the specifications of this standard is encouraging. Furthermore, BS ISO 2184 provides valuable guidelines for supplementary testing, such as water vapour permeability, water absorption, and dimensional stability under elevated temperatures, which are crucial for assessing the suitability of these materials as building components.

4.6. End of life

To assess end-of-life pathways, two studies were conducted to determine the potential for recyclability and biodegradation. The recyclability of the Xanthan foam was evaluated by a process designed to recover the cellulosic fibres and recreate the foam with minimal loss in performance, adapted from [27]. Foam samples were submerged in 200 grams of water and soaked for 2 min to dissolve the hydrophilic binder, allowing the separation of the fibres. The excess water was then strained, and the recovered pulp was combined with new xanthan gum, SDS, borax and water to replicate the initial foaming process. This recycling method was repeated over three cycles, with measurements of density and thermal conductivity taken at each stage. Results showed that the foam maintained its structural integrity and functional properties, with only a 5%-6% reduction in density and a 12.8% increase in thermal conductivity (see Table 1). These changes are attributed to the incomplete removal of additives and slight fibre loss, indicating that the foam can be effectively recycled with minimal degradation in performance. In contrast, attempts to recycle the boratebased foam were unsuccessful, as the foam collapsed upon drying. This outcome aligns with previous studies on chemically cross-linked foams, where the depletion of active reaction sites during initial foam creation prevents successful recycling [86,87].

Table 1
Results from recycling test of Xanthan foam.

	Initial	Round 1	Round 2	Round 3
Density (kg/m³)	21.1	20.4	19.9	19.7
Thermal Conductivity (W/m*K)	0.0421	0.0432	0.0453	0.0475

The biodegradability of the foams was assessed through a soil burial test. Cylindrical specimens of diameter 50 mm, height 12 mm for the Borate and 6 mm for the Xanthan sample, and common initial mass 0.25 g, were buried in commercially available topsoil in sealed containers for 28 days, at a temperature of 27 °C, and 65% air humidity, to measure mass loss due to microbial degradation. The Xanthan and Borate foams experienced mass losses of 26.5% and 23.7%, respectively. Soil burial tests of cellulose composite foams show a significantly larger mass loss of 96.6% [88]. The reduced degradation rate of the developed foams of this study is likely due to the presence of lignin in the constituent fibres, which inhibits enzymatic breakdown by slowing cellulase diffusion [89], and borax, which has antibacterial and antifungal properties that further inhibit microbial activity [90].

4.7. Life cycle assessment

A life cycle analysis covering cradle-to-gate system boundaries was conducted for the two foams to identify key emission hot spots and compare environmental impacts against traditional insulation materials. The methodology of ISO 14040 standard [42] was followed, and consists of the following stages: raw material acquisition, transportation, and manufacturing. Calculations were performed using the OpenLCA software [91] with the EcoInvent v3.10 and Agrybalyse v3.1.1 databases. For each material, the mass corresponding to a functional unit of thermal resistance per unit area (R-value) equal to 1 $\rm m^2 K/W$ was specified; this was 460 g and 886 g for the Borate and Xanthan foams, respectively.

Due to a lack of data for specific chemicals and local practices, proxies were used for the cultivation of henequen and the production of xanthan gum and SDS. As is common in such studies, the intent is to provide a benchmark comparison with general classes of the above materials. Detailed assumptions, limitations and inventory are listed in Supplemental Materials.

We first compare the life cycle impacts of the two foams of this study. The results indicated that the equivalent CO_2 emissions per functional unit were 7.62 kg and 3.81 kg for the Xanthan and Borate foams, respectively. The primary emission source for both foams is the diesel burnt in the agricultural practices and cultivation of the agave plant, which contributes 55% and 30% of the total emissions for the Xanthan and Borate foams, respectively. The electricity used in the manufacturing process also accounts for a significant proportion of emissions, approximately 30% and 50% for the Xanthan and Borate foams, respectively.

The differences in the emissions outputs of the two foams are primarily due to the raw henequen fibre consumption; the ratio of fibre mass per functional unit of the Borate and Xanthan foams is 1:1.9. The emissions associated with the manufacturing of the remaining foam constituents account for 15% and 20% for the Xanthan and Borate foams respectively, while transportation and waste produced are insignificant (in the order of 0.28% due to the only waste stream during production being wastewater treatment).

Next, we discuss the relative comparison in several environmental impact categories of the foams developed herein to other insulation materials: Polyurethane Foams (PUR), Expanded Polystyrene Foams (EPS), Glass Wool, and Cellulose Foams (from waste paper (post consumer) and chemical additives). Twelve impact categories are considered. These are: terrestial acidification potential (TAP), global warming potential over 500 years (GWP500), particulate matter formation potential (PMFP), ozone depletion potential (ODP), human toxicity

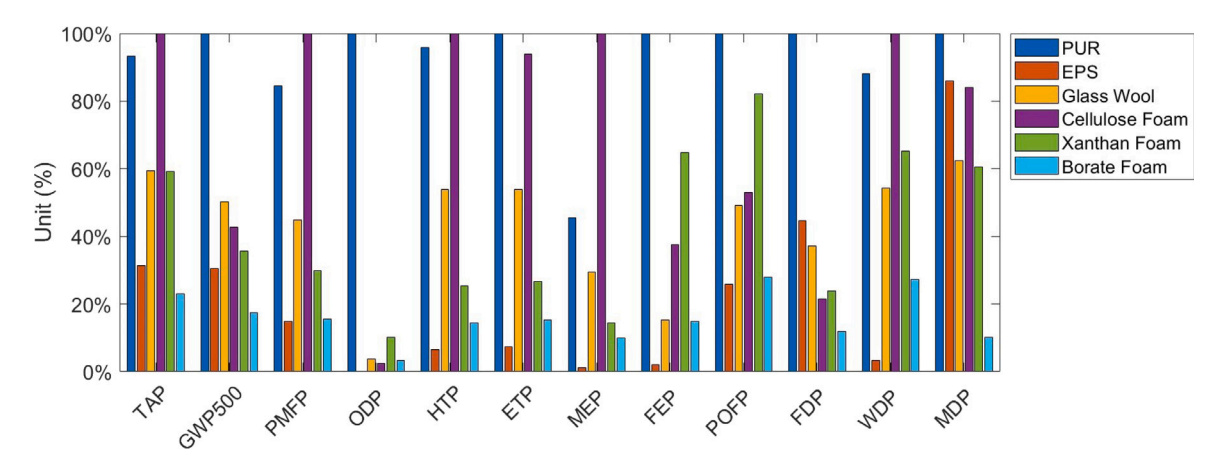


Fig. 14. Normalised environmental impacts of Borate and Xanthan foams compared to Cellulose Foam, Glass Wool, EPS, and PUR foams.

potential (HTP), ecotoxicity potential (ETP) (sum of freshwater, marine, and terrestial), marine eutrophication potential (MEP), freshwater eutrophication potential (FEP), photochemical oxidant formation potential (POFP), fossil depletion potential (FDP), water depletion potential (WDP) and metal depletion potential(MDP). The results, presented in Fig. 14, are normalised by the highest output in each category.

Selecting as an initial benchmark for comparative discussion PUR foams, an inexpensive material for thermal insulation, it is observed that the fibrous foams developed here reduce the environmental impact in all categories. Notably, in toxicity categories (HTP and ETP), Xanthan and Borate foams reduce impacts by up to 73.4% and 84.9%, respectively, compared to the PUR foams. The Borate foam exhibits the lowest global warming potential (GWP500), 82.5% lower than PUR. Both foams also show reduced fossil fuel depletion (FDP) by 88.2% and 76.0%, respectively, for Borate and Xanthan foams, respectively. Water use (WU) is 89.9% lower for borate foam compared to PUR, though xanthan foam shows a more modest reduction of 39.4%.

Comparison with glass wool, a high performance material for thermal insulation, reveals that improvements can be achieved in most categories, except for three categories: (1) FEP due to the inorganic composition of glass wool which lacks nutrients that contribute to algal blooms in freshwater ecosystems [92–94], (2) POFP due to the minimal release of volatile organic compounds during manufacturing, which reduces the formation of photochemical oxidants [95], and (3) WDP due to the low water usage of glass wool manufacturing compared to the foams of this study [95] (used primarily in the fibrillation and liquid foaming parts of the process). The life cycle improvements outlined above can be attributed primarily to the simple and low-energy fibre extraction and manufacturing processes.

5. Conclusions

This study demonstrated the successful fabrication of lightweight, fibrous foams from lignocellulosic henequen fibres, using simple and energy-efficient processing techniques. Agitative blending effectively fibrillated the raw fibres, significantly reducing their mean diameter and increasing their surface area. This enhanced surface area facilitated the formation of stable fibrous networks through physical interconnections, the addition of Xanthan gum, or chemical cross-linking via borate ester bonds.

Both the Xanthan and Borate foams exhibited promising thermal insulation properties with low thermal conductivity (42 mW/m*K and 43 mW/m*K respectively), low apparent densities (21.0 kg/m³ and 11.5 kg/m³ respectively), and high compressive stiffness (56 kPa and 19 kPa, respectively). Notably, the Xanthan foam demonstrated excellent recyclability, maintaining its performance even after three recycling cycles. Furthermore, both foams exhibited inherent fire resistance with a limited oxygen index (LOI) of 29.5% for both.

Life cycle assessment results indicated that both foams possess lower environmental impacts compared to conventional insulation materials such as polyurethane and glass wool, across most assessment categories. These findings suggest that the developed henequen-based foams offer a sustainable and competitive alternative to existing thermal insulation materials, with potential applications in various sectors.

CRediT authorship contribution statement

Qasim Shoaib: Writing – review & editing, Writing – original draft, Visualization, Validation, Methodology, Investigation, Formal analysis, Data curation. Vaidurya Mukherjee: Writing – review & editing, Writing – original draft, Visualization, Validation, Methodology, Investigation, Formal analysis, Data curation. Vasiliki Marmaridou: Writing – review & editing, Writing – original draft, Visualization, Validation, Software, Methodology, Investigation, Formal analysis. Aleksei Sereda: Writing – review & editing, Writing – original draft, Visualization, Validation, Validation, Resources, Methodology, Investigation, Formal analysis. Peterasp Nawzar Satarawala: Writing – review & editing, Writing – original draft, Visualization, Methodology, Investigation, Formal analysis. Jose G. Carrillo: Writing – review & editing, Resources, Funding acquisition, Conceptualization. Eral Bele: Writing – review & editing, Supervision, Resources, Project administration, Investigation, Funding acquisition, Formal analysis, Conceptualization.

Declaration of competing interest

The authors declare that they have no known competing financial interests or personal relationships that could have appeared to influence the work reported in this paper.

Acknowledgements

This research was partly supported by the Royal Society International Exchanges Scheme 2020, Mexico (Grant No. IES/R1/201026). One of the authors (JGC) was also supported by the Consejo Nacional de Humanidades Ciencias *y* Tecnologías de Mexico (CONAHCYT) through the project Ciencia Básica 2017–2018 (Grant No. A1-S- 8864). The authors are grateful for the technical support provided by Dr Luna Jiang in the acquisition of SEM micrographs and CT scans, and for the productive discussions with Dr Vikramjeet Singh, in the Department of Mechanical Engineering, University College London.

Appendix A. Supplementary data

Supplementary material related to this article can be found online at https://doi.org/10.1016/j.mtsust.2025.101111.

Data availability

Data will be made available on request.

References

- [1] Building materials and the climate: constructing a new future, 2023, [Online]; Available from: https://wedocs.unep.org/20.500.11822/43293. (Accessed May 2024)
- [2] 2022 global status report for buildings and construction, 2022, [Online];Available from: https://www.unep.org/resources/publication/2022-global-status-report-buildings-and-construction. (Accessed May 2024).
- [3] A. Rempher, R. Esau, M. Weir, Embodied Carbon 101: Building Materials, Carbon Leadership Forum, 2020, [Online]; Available from: https://carbonleadershipforum.org/embodied-carbon-101/. (Accessed May 2024).
- [4] M. Kymäläinen, One Click LCA Construction LCA Bootcamp, One Click LCA Academy, 2023.
- [5] P. Jaureguiberry, N. Titeux, M. Wiemers, D. Bowler, L. Coscieme, A.S. Golden, C.A. Guerra, U. Jacob, Y. Takahashi, J. Settele, S. Díaz, Z. Molnár, A. Purvis, The direct drivers of recent global anthropogenic biodiversity loss, Sci. Adv. 8 (2022).
- [6] J. Michalak, S. Czernik, M. Marcinek, B. Michałowski, Environmental burdens of external thermal insulation systems. Expanded polystyrene vs. Mineral wool: Case study from Poland, Sustainability (2020).
- [7] M.G. Muluneh, Impact of climate change on biodiversity and food security: a global perspective—a review article, Agric. Food Secur. 10 (2021).
- [8] Z. Chen, Q. Feng, R. Yue, Z. Chen, O. Moselhi, A. Soliman, A. Hammad, C. An, Construction, renovation, and demolition waste in landfill: a review of waste characteristics, environmental impacts, and mitigation measures, Environ. Sci. Pollut. Res. 29 (31) (2022) 46509–46526.
- [9] Global waste management outlook 2024: Beyond an age of waste Turning rubbish into a resource, 2024, Available from: https://wedocs.unep.org/20.500. 11822/44939.
- [10] Z. Zhang, F. Hao, D. Hu, W. Liu, X. Chen, Natural plant fiber-based materials for packaging applications – a review of recent innovations and developments, Adv. Mater. Technol. (2024).
- [11] S. Mehrzad, E. Taban, P. Soltani, S.E. Samaei, A. Khavanin, Sugarcane bagasse waste fibers as novel thermal insulation and sound-absorbing materials for application in sustainable buildings, Build. Environ. 211 (2022) 108753.
- [12] Y. Zhu, Z. Yu, J. Zhu, Y. Zhang, X. Ren, F. Jiang, Developing flame-retardant lignocellulosic nanofibrils through reactive deep eutectic solvent treatment for thermal insulation, Chem. Eng. J. 445 (2022) 136748.
- [13] R. Neagu, M. Cuénoud, P. Bourban, F. Berthold, E. Gamstedt, M. Lindström, J. Månson, The potential of wood fibers as reinforcement in cellular biopolymers standard, Submitt. J. Cell. Plast. (2011).
- [14] L. Liu, Z. Yuan, X. Fan, C. Pan, X. Li, A review of interfacial bonding mechanism of bamboo fiber reinforced polymer composites. Cellulose (2021) 1–18.
- [15] S. Tangjuank, Thermal insulation and physical properties of particleboards from pineapple leaves, Int. J. Phys. Sci. 6 (2011) 4528–4532.
- [16] X. Chen, J. Li, H. Essawy, A. Pizzi, E. Fredon, C. Gerardin, G. Du, X. Zhou, Flame-retardant and thermally-insulating tannin and soybean protein isolate (SPI) based foams for potential applications in building materials, Constr. Build. Mater. 315 (2022) 125711, Available from: https://www.sciencedirect.com/science/article/pii/S0950061821034450.
- [17] K.Y. Lee, L.L.C. Wong, J.J. Blaker, J.M. Hodgkinson, A. Bismarck, Bio-based macroporous polymer nanocomposites made by mechanical frothing of acrylated epoxidised soybean oil, Green Chem. 13 (11) (2011) 3117–3123.
- [18] F. Rosas-Díaz, D.G. García-Hernández, C.A. Juárez-Alvarado, Development of lignocellulosic-based insulation materials from agave fourcroydes and Washingtonia filifera for use in sustainable buildings, Sustainability 16 (13) (2024) Available from: https://www.mdpi.com/2071-1050/16/13/5455.
- [19] H. Malekzadeh, N. Md Zaid, E. Bele, Characterization and structural properties of bamboo fibre solid foams, Cellulose 28 (2) (2021) 703–714.
- [20] C.C.N. Martins, M.C. Dias, M.C. Mendonça, A.F.S. Durães, L.E. Silva, J.R. Félix, R.A.P. Damásio, G.H.D. Tonoli, Optimizing cellulose microfibrillation with NaOH pretreatments for unbleached Eucalyptus pulp, Cellulose 28 (2021) 11519–11531.
- [21] Y. Zhu, J. Zhu, Z. Yu, Y. Ye, X. Sun, Y. Zhang, P. Zhu, F. Jiang, Air drying scalable production of hydrophobic, mechanically stable, and thermally insulating lignocellulosic foam, Chem. Eng. J. 450 (2022) 138300, Available from: https://www.sciencedirect.com/science/article/pii/S1385894722037834.
- [22] R. Mort, K. Vorst, G. Curtzwiler, S. Jiang, Biobased foams for thermal insulation: material selection, processing, modelling, and performance, RSC Adv. 11 (2021) 4375–4394, http://dx.doi.org/10.1039/D0RA09287H, Available from.
- [23] P. Wang, N. Aliheidari, X. Zhang, A. Ameli, Strong ultralight foams based on nanocrystalline cellulose for high-performance insulation, Carbohydr. Polymers 218 (2019) 103–111, Available from: https://www.sciencedirect.com/science/ article/pii/S0144861719304527.

- [24] S.C. Li, B.C. Hu, Y.W. Ding, H.W. Liang, C. Li, Z.Y. Yu, Z.Y. Wu, W.S. Chen, S.-H. Yu, Wood-derived ultrathin carbon nanofiber aerogels, Angew. Chem. Int. Ed. 57 (24) (2018) 7085–7090, Available from: https://onlinelibrary.wiley.com/doi/abs/10.1002/anie.201802753.
- [25] L. Lujan, M.L. Goñi, R.E. Martini, Cellulose–chitosan biodegradable materials for insulating applications, ACS Sustain. Chem. Eng. 10 (36) (2022) 12000–12008, http://dx.doi.org/10.1021/acssuschemeng.2c03538, Available from.
- [26] Y. Li, V.A. Tanna, Y. Zhou, H.H. Winter, J.J. Watkins, K.R. Carter, Nanocellulose aerogels inspired by frozen tofu, ACS Sustain. Chem. Eng. 5 (8) (2017) 6387–6391.
- [27] L. Chen, S. Wang, S. Wang, C. Chen, L. Qi, L. Yu, Z. Lu, J. Huang, J. Chen, Z. Wang, et al., Scalable production of biodegradable, recyclable, sustainable cellulose–mineral foams via coordination interaction assisted ambient drying, ACS Nano 16 (10) (2022) 16414–16425.
- [28] Z. Atoufi, K.S. Gordeyeva, M.F. Cortes Ruiz, P.A. Larsson, L.W. gberg, Syner-gistically stabilized wet foams from heat treated β-lactoglobulin and cellulose nanofibrils and their application for green foam production, Appl. Mater. To-day 39 (2024) 102251, Available from: https://www.sciencedirect.com/science/article/pii/\$2352940724001963.
- [29] N. Lavoine, L. Bergström, Nanocellulose-based foams and aerogels: processing, properties, and applications, J. Mater. Chem. A 5 (2017) 16105–16117, http://dx.doi.org/10.1039/C7TA02807E, Available from.
- [30] Y. Zhou, W. Yin, Y. Guo, C. Qin, Y. Qin, Y. Liu, Green preparation of lightweight, high-strength cellulose-based foam and evaluation of its adsorption properties, Polymers 15 (8) (2023) Available from: https://www.mdpi.com/2073-4360/15/ 8/1879.
- [31] V. da Costa Correia, A.A. da Silva Curvelo, K. Marabezi, A.E.F. de Souza Almeida, H.S. Junior, Bamboo cellulosic pulp produced by the ethanol/water process for reinforcement applications, Cienc. Florest. 25 (2015) 127–135, Available from: https://api.semanticscholar.org/CorpusID:54752144.
- [32] Agave fourcroydes (henequen), CABI Compend. (2022) http://dx.doi.org/10. 1079/cabicompendium.3853, Available from.
- [33] K. Seeniappan, L. Natrayan, Surface Modification of Henequen Fibers with Catalyst for Improving Mechanical and Thermal Properties in Phenolic Composites for Automotive Uses, 2024, SAE Technical Paper.
- [34] F.X. Espinach, F. Julian, M. Alcalà, F. Vilaseca, F. Carrasco, P. Mutjé, Effective tensile strength estimation of natural fibers through micromechanical models: The case of henequen fiber reinforced-PP composites, Polymers 14 (22) (2022) Available from: https://www.mdpi.com/2073-4360/14/22/4890.
- [35] P. Yasin, M. Venkata Ramana, C. Krishna Vamshi, K. Pradeep, A study of continuous Henequen/Epoxy composites, Mater. Today: Proc. 18 (2019) 3798–3811, 9th International Conference of Materials Processing and Characterization, ICMPC-2019, Available from: https://www.sciencedirect.com/science/article/pii/S2214785319324976.
- [36] A. Shalwan, T. Alajmi, N. Alajmi, Study on sisal fibres as insulator in building materials, Glob. J. Eng. Technol. Adv. 15 (2) (2023) 124–140.
- [37] J.d. Melo Filho, F.d. Silva, R.D. Toledo Filho, Degradation kinetics and aging mechanisms on sisal fiber cement composite systems, Cem. Concr. Compos. 40 (2013) 30–39, Available from: https://www.sciencedirect.com/science/article/ pii/S0958946513000504.
- [38] S. Ouhaibi, O. Mrajji, A.G. M. El Wazna, N. Belouaggadia, M. Ezzine, R. Lbibb, A.E. Bouari, O. Cherkaoui, Sisal-fibre based thermal insulation for use in buildings, Adv. Build. Energy Res. 16 (4) (2022) 489–513, http://dx.doi.org/10.1080/17512549.2021.1982768, Available from.
- [39] J.F. Castillo-Lara, E.A. Flores-Johnson, A. Valadez-Gonzalez, P.J. Herrera-Franco, J.G. Carrillo, P.I. Gonzalez-Chi, Q.M. Li, Mechanical properties of natural fiber reinforced foamed concrete, Materials 13 (14) (2020) Available from: https://www.mdpi.com/1996-1944/13/14/3060.
- [40] R. Sescousse, R. Gavillon, T. Budtova, Aerocellulose from cellulose-ionic liquid solutions: Preparation, properties and comparison with cellulose-NaOH and cellulose-NMMO routes, Carbohydr. Polymers 83 (4) (2011) 1766-1774.
- [41] T. Yimer, A. Gebre, Effect of fiber treatments on the mechanical properties of sisal fiber-reinforced concrete composites, Adv. Civ. Eng. 2023 (1) (2023) 2293857.
- [42] International Organization for Standardization, Environmental Management Life Cycle Assessment — Principles and Framework, International Organization for Standardization, Geneva, Switzerland, 2006, ISO 14040:2006.
- [43] A. Acero, C. Rodríguez, A. Changelog, LCIA Methods Impact Assessment Methods in Life Cycle Assessment and their Impact Categories, GreenDelta, 2015, Available from: https://www.openlca.org/wp-content/uploads/2015/11/ LCIA-METHODS-v.1.5.4.pdf.
- [44] S. Mortimer, A. Peguy, The influence of air-gap conditions on the structure formation of lyocell fibers, J. Appl. Polym. Sci. 60 (10) (1996) 1747–1756.
- [45] W. Udomkichdecha, S. Chiarakorn, P. Potiyaraj, Relationships between fibrillation behavior of lyocell fibers and their physical properties, Text. Res. J. 72 (11) (2002) 939–943.
- [46] W. Zhang, S. Okubayashi, W. Badura, T. Bechtold, Fibrillation tendency of cellulosic fibers, part 6: Effects of treatments with additive polymers, J. Appl. Polym. Sci. 101 (6) (2006) 4140–4147.

- [47] E. Bisanda, M.P. Ansell, Properties of sisal-CNSL composites, J. Mater. Sci. 27 (1992) 1690–1700.
- [48] H.E. Gram, Durability of Natural Fibres in Concrete, Swedish Cement and Concrete Research Institute, Stockholm, 1984.
- [49] Y. Ma, M. Rissanen, X. You, K. Moriam, M. Hummel, H. Sixta, New method for determining the degree of fibrillation of regenerated cellulose fibres, Cellulose 28 (2021) 31–44.
- [50] E.S. Ferreira, C.A. Rezende, E.D. Cranston, Fundamentals of cellulose lightweight materials: bio-based assemblies with tailored properties, Green Chem. 23 (10) (2021) 3542–3568.
- [51] J.S. Fabiyi, B.M. Ogunleye, Mid-infrared spectroscopy and dynamic mechanical analysis of heat-treated obeche (Triplochiton scleroxylon) wood, Maderas Cienc. Tecnol. A 17 (1) (2015) 05–16.
- [52] V. Apostolopoulou-Kalkavoura, P. Munier, L. Bergström, Thermally insulating nanocellulose-based materials, Adv. Mater. 33 (28) (2021) 2001839.
- [53] Z. Pásztory, et al., An overview of factors influencing thermal conductivity of building insulation materials, J. Build. Eng. 44 (2021) 102604.
- [54] V. Hospodarova, E. Singovszka, N. Stevulova, Characterization of cellulosic fibers by FTIR spectroscopy for their further implementation to building materials, Am. J. Anal. Chem. 9 (6) (2018) 303–310.
- [55] F. Xu, J. Yu, T. Tesso, F. Dowell, D. Wang, Qualitative and quantitative analysis of lignocellulosic biomass using infrared techniques: a mini-review, Appl. Energy 104 (2013) 801–809.
- [56] S. He, C. Liu, X. Chi, Y. Zhang, G. Yu, H. Wang, B. Li, H. Peng, Bio-inspired lightweight pulp foams with improved mechanical property and flame retardancy via borate cross-linking, Chem. Eng. J. 371 (2019) 34–42.
- [57] G. Yang, J. Zhao, L. Cui, S. Song, S. Zhang, L. Yu, P. Zhang, Tribological characteristic and mechanism analysis of borate ester as a lubricant additive in different base oils, RSC Adv. 7 (13) (2017) 7944–7953.
- [58] J. Han, Y. Yue, Q. Wu, C. Huang, H. Pan, X. Zhan, C. Mei, X. Xu, Effects of nanocellulose on the structure and properties of poly (vinyl alcohol)-borax hybrid foams, Cellulose 24 (2017) 4433–4448.
- [59] S. Tanpichai, F. Phoothong, A. Boonmahitthisud, Superabsorbent cellulose-based hydrogels cross-liked with borax, Sci. Rep. 12 (1) (2022) 8920.
- [60] W. Ge, S. Cao, F. Shen, Y. Wang, J. Ren, X. Wang, Rapid self-healing, stretchable, moldable, antioxidant and antibacterial tannic acid-cellulose nanofibril composite hydrogels, Carbohydr. Polymers 224 (2019) 115147.
- [61] Y. Jia, S. Gao, Y. Jing, Y. Zhou, S. Xia, FTIR spectroscopy of magnesium tetraborate solution, Chem. Pap 55 (3) (2001) 162–166.
- [62] F. Chatti, D. Poquillon, C. Bouvet, G. Michon, Numerical modelling of entangled carbon fibre material under compression, Comput. Mater. Sci. 151 (2018) 14–24, Available from: https://www.sciencedirect.com/science/article/pii/S0927025618302866.
- [63] M. Islam, G. Tudryn, R. Bucinell, L. Schadler, R. Picu, Morphology and mechanics of fungal mycelium, Sci. Rep. 7 (2017) 13070.
- [64] M. Alimadadi, S. Lindström, A. Kulachenko, Role of microstructures in the compression response of three-dimensional foam-formed wood fiber networks, Soft Matter 14 (2018).
- [65] BSI ISO 21844:2018. Cellular Plastic Cellulose Foam Thermal Insulation Material Specification (UK implementation), BSI (British Standards Institution), Geneva. Switzerland. 2018.
- [66] Uses of Borates in Flame Retardants, American Borate Company, 2019, [Online]; Available from: http://www.americanborate.com/all-about-borates/borate-applications/borates-in-flame-retardants/. (Accessed May 2024).
- [67] American Society for Testing and Materials, Standard Test Method for Measuring the Minimum Oxygen Concentration to Support Candle-Like Combustion of Plastics (Oxygen Index), American Society for Testing and Materials, Philadelphia, USA, 2023, ASTM D2863-19.
- [68] M. Nelson, H. Sidhu, R. Weber, G. Mercer, A dynamical systems model of the limiting oxygen index test, ANZIAM J. 43 (1) (2001) 105–117.
- [69] G. Schinazi, E.J. Price, D.A. Schiraldi, Fire testing methods of bio-based flameretardant polymeric materials, in: Bio-Based Flame-Retardant Technology for Polymeric Materials, Elsevier, 2022, pp. 61–95.
- [70] A. Horrocks, M. Ugras, The persistence of burning of textiles in different oxygen environments and the determination of the extinction oxygen index, Fire Mater. 7 (3) (1983) 111–118.
- [71] B. Hedskog, F. Ryber, The Classification System for Surface Lining Materials used in Buildings in Europe and Japan, 1998, Student Paper.
- [72] P. Blomqvist, M. Simonson, P. Thureson, Compilation of international building regulations (Fire) relevant for EPS/XPS, 2010.

- [73] A. Korjenic, V. Petránek, J. Zach, J. Hroudová, Development and performance evaluation of natural thermal-insulation materials composed of renewable resources, Energy Build. 43 (9) (2011) 2518–2523.
- [74] M. Schulte, I. Lewandowski, R. Pude, M. Wagner, Comparative life cycle assessment of bio-based insulation materials: Environmental and economic performances, GCB Bioenergy 13 (6) (2021) 979–998.
- [75] STEICO, STEICOflex 036 flexible thermal insulation [product information], 2018, Available from: https://www.steico.com/en/products/insulation/insulation-between-studs/flexible-thermal-insulation/steicoflex-036. (Accessed 2 September 2024).
- [76] Kenaf Fiber, Soundproofing and thermal insulation material in natural fibers for green building, 2024, Available from: https://www.kenaf-fiber.com/en/isolkenaf. html. (Accessed 2 September 2024).
- [77] Kenaf Fiber, Floor soundproofing and thermal insulation rolls in kenaf natural fibers, 2024, Available from: https://www.kenaf-fiber.com/en/isolkenaf-pav.html. (Accessed 2 September 2024).
- [78] ROCKWOOL, Thermalrock S (slab) data sheet, 2024, Available from: https: //www.rockwool.com/siteassets/rw-in/product-documentation/products/data-sheets/thermalrock-s-data-sheet_in.pdf. (Accessed 2 September 2024).
- [79] Knauf Insulation, Glass Mineral Wool Insulation 0.034 -0.035 W/mK Environmental Product Declaration, Knauf Insulation, 2019, EPD-KNI-20190031-CBC2-EN.
- [80] E. Elsacker, S. Vandelook, J. Brancart, E. Peeters, L. De Laet, Mechanical, physical and chemical characterisation of mycelium-based composites with different types of lignocellulosic substrates, PLoS One 14 (7) (2019) e0213954.
- [81] M.P. Jones, A. Mautner, S. Luenco, A. Bismarck, S. John, Engineered mycelium composite construction materials from fungal biorefineries: A critical review, Mater. Des. (2019) 108397.
- [82] Z. Zhang, F. Hao, D. Hu, W. Liu, X. Chen, Natural plant fiber-based materials for packaging applications—A review of recent innovations and developments, Adv. Mater. Technol. (2024) 2401020.
- [83] J. Liao, P. Luan, Y. Zhang, L. Chen, L. Huang, L. Mo, J. Li, Q. Xiong, A lightweight, biodegradable, and recyclable cellulose-based bio-foam with good mechanical strength and water stability, J. Environ. Chem. Eng. 10 (3) (2022) 107788.
- [84] Y. Hou, J. Liao, L. Huang, S. Guo, Y. Zhang, Z. Liu, L. Mo, X. Zhang, J. Li, Plant bio-inspired laminar cellulose-based foam with flame retardant, thermal insulation and excellent mechanical properties, J. Mater. Chem. A 11 (3) (2023) 1138–1147.
- [85] I. Hafez, M. Tajvidi, Comprehensive insight into foams made of thermomechanical pulp fibers and cellulose nanofibrils via microwave radiation, ACS Sustain. Chem. Eng. 9 (30) (2021) 10113–10122, Available from.
- [86] J. Liao, Y. Hou, J. Li, M. Zhang, Y. Dong, X. Chen, Lightweight and recyclable hybrid multifunctional foam based cellulose fibers with excellent flame retardant, thermal, and acoustic insulation property, Compos. Sci. Technol. 244 (2023) 110315.
- [87] P. Nechita, S.M. Năstac, Overview on foam forming cellulose materials for cushioning packaging applications, Polymers 14 (10) (2022) 1963.
- [88] D. Wu, M. Wang, W. Yu, G.G. Wang, J. Zhang, A robust, biodegradable and recyclable all-cellulose ionogel from low-value wood, Chem. Eng. J. (2024) 150121.
- [89] M.Q. Zhang, M.Z. Rong, X. Lu, Fully biodegradable natural fiber composites from renewable resources: all-plant fiber composites, Compos. Sci. Technol. 65 (15–16) (2005) 2514–2525.
- [90] H.S. Coskun, L. Kehribar, S. Surucu, M. Aydin, M. Mahirogullari, H.S. Coşkun, L. Kehribar Sr, M. Aydın, M. Mahiroğulları, Antibacterial effects of sodium borate and calcium borate based polymeric coatings for orthopedic implants, Cureus 14 (2) (2022).
- [91] GreenDelta, openLCA, 2023, Available from: https://www.openlca.org. (Accessed 11 April 2024).
- [92] S. Zidd, S. Kidd, R. Simpson, Prevention of Harmful Algal Blooms by the Mitigation of Phosphorus Nutrient Loading via Filtration by Steel Wool and Activated Carbon, Williams Honors College, Honors Research Projects, 2020, Available from: https://ideaexchange.uakron.edu/honors/research_projects/877.
- [93] Z. Chen, T. Liu, Development and application status of glass wool, rock wool, and ceramic wool, in: Thermal Insulation and Radiation Control Technologies for Buildings, Springer, 2022, pp. 129–161.
- [94] H. Paerl, J.T. Scott, Throwing fuel on the fire: synergistic effects of excessive nitrogen inputs and global warming on harmful algal blooms, Environ. Sci. Technol. 44 20 (2010) 7756–7758.
- [95] C. Zhao, Y. Liu, S. Ren, Y. Zhang, Life cycle assessment of typical glass wool production in China, Mater. Sci. Forum 913 (2018) 998–1003.